Journal of Mobile Multimedia, Vol. 8, No. 2 (2012) 088–104

ANALYSIS OF FIELD INTENSITY DISTRIBUTION IN INHOMOGENEOUS PROPAGATION ENVIRONMENT BASED ON TWO-RAY MODEL

JUNICHI HONDA
Surveillance and Communications Department, Electronic Navigation Research Institute
Cyofu, 182-0012 Japan
jhonda.fit@gmail.com

KAZUNORI UCHIDA MASAFUMI TAKEMATSU
Department of Intelligent Information System Engineering, Fukuoka Institute of Technology
Fukuoka, 811-0295 Japan
k-uchida@fit.ac.jp

Received November 1, 2011
Revised May 19, 2012

This paper is concerned with an analysis of field intensity distribution caused by sensor nodes located on inhomogeneous terrestrial surfaces. First, we introduce 1-ray and 2-ray models with two modification factors to estimate the field intensity distribution. One of the two factors is an amplitude modification (α) and the other is a distance order of propagation (β). By using the two factors, we can calculate field intensity distributions in complicated natural environment such as random rough surface. Then, we propose an estimation formula for analyzing electric fields in inhomogeneous propagation environments based on the conventional two models. Next we introduce an algorithm for radio communication distance based on the 1-ray and 2-ray models. In the numerical examples, we show the field intensity distribution caused by sensor nodes located randomly on inhomogeneous terrestrial surfaces, using 2-ray models. Finally, we discuss how many sensor nodes are needed to cover the field area in order to construct networks.

Keywords: field intensity distribution; sensor network; 1-ray model; 2-ray model; modification factor; amplitude modification; distance order of propagation; density of sensor node; communication distance; inhomogeneous propagation environment
Communicated by: D. Taniar

1 Introduction

The information and communication technologies play an important role in the modern society, and many researchers are working on establishing the ubiquitous networks. Recently, the sensor network technologies [2] among many wireless communication systems have attracted many researchers' interest. The sensor devices equipped with antenna collect many physical information and construct networks by communicating themselves automatically. The studies of sensor networks are discussed mainly from the view points of network layer of OSI model and MAC [3, 4]. Those studies assume that every sensor can communicate with each other by radio waves, however, wireless devices sometimes fail to receive desired signals by scattered waves from obstacles located on the terrestrial surfaces. And, in the radio engineering field to develop the wireless devices such as circuit and antenna, it is severely required to estimate the behavior of electromagnetic waves in complicated propagation

environments, besides the discussion of network layer.

The sensor devices are usually distributed not only in closed spaces but also in open spaces such as complicated propagation environments like dessert, hilly terrain, forest, vegetable fields, sea surface and so on. Since their terrestrial surfaces are considered to be statistically random, the radio waves emitted from the sensor devices are much more influenced by diffused reflections from Random Rough Surfaces (RRSs). Therefore, it is important to investigate the propagation characteristics along RRSs in order to construct an efficient and reliable sensor network system [5]. And it is also important to estimate the field intensity distribution above RRSs and to acquire knowledge how many sensors are needed to construct networks. The purpose of this paper is to numerically investigate the electric field distribution above a terrestrial surface by using simple numerical methods and to consider how many sensor nodes are needed to construct efficient networks.

There are some numerical methods such as Finite Difference Time Domain (FDTD) method [6], Kirchhoff approximation [7], perturbation method [8] and Ray-Tracing Method (RTM), for analyzing electromagnetic field distribution and backscattering from RRSs. One of them, the RTM is widely used for computation of electric fields in large scale of propagation problems, but it requires much computation time for ray searching between source and receiver and for finding reflection and diffraction points. Due to this big problem, we proposed a Discrete Ray Tracing Method (DRTM) to compute electric fields above RRSs as quickly as possible [9, 10]. Using this proposed method, we investigated the relationship between propagation characteristics along RRSs and the shapes of RRSs.

The DRTM would be one of suitable numerical technique and its computation time is much shorter than that of the conventional RTM. However, it is difficult for the general computer to compute electric field due to the computation of ray searching, when we treat very long RRSs and 2D RRSs. Therefore, we proposed two numerical methods based on 1-ray and 2-ray models with two modification factors [11]. Two numerical methods are so simple and applied to numerical computation of electric field in the free space and above a plane-ground, respectively. To deal with the electric field distribution in complicated propagation environments, we have introduced two modification factors into 1-ray and 2-ray models [11]. One of two factors is an amplitude modification (α), and the other is a distance order of propagation (β). Using two parameters, we can estimate the field distribution in complicated environments. It has also been found that two modifications depend on the surfaces' shape and antenna height, operating frequency and material constants [12]. It is easy to determine the two modifications by comparing with the numerical results obtained by the DRTM. We have so far investigated the relationship between two modifications and RRS's configurations which are generated by a correlation length (cl) and a deviation of surfaces' height (h), when the source and receiver are located close to RRS.

In this paper, using 1-ray and 2-ray models with α and β, we investigate the field intensity distribution caused by sensors located on RRSs, whose structures are assumed to be inhomogeneous. First, we introduce 1-ray and 2-ray models with α and β which can estimate the field intensities in complicated propagation environments such as urban, suburban, rural areas and RRSs. Two numerical methods have been applied so far to field estimation above homogeneous RRSs which mean that RRSs are given by constant parameters cl and h. Therefore, we propose a modified algorithm of 1-ray and 2-ray models to treat more complicated RRSs, that is, inhomogeneous RRSs.

Next, we introduce an estimation formula of radio communication distance based on the 1-ray and 2-ray models. This formula enables us to easily compute the communication distance of wireless devices. Finally, we show some numerical examples of field intensity distribution as well as the

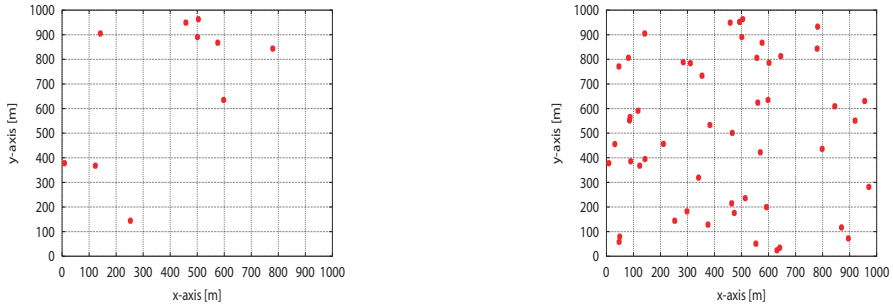

(a) Number of node = 10. (b) Number of node = 50.

Fig. 1. Random allocation of sensor nodes.

communication length of sensor node. From numerical results, we discuss how many sensor nodes are needed to construct networks in inhomogeneous propagation environments.

2 1-Ray and 2-ray Models

In general, 1-ray model is applied to the field estimation in the free space, and 2-ray model is applied to it above a plane-ground. Therefore, we introduce two models with two modification factors to calculate electric field intensity in complicated natural environment. In this paper, we calculate the field intensity distribution caused by sensor nodes located on the terrestrial surface. First we propose the random allocation method of sensor nodes. Next, we introduce two numerical methods based on the 1-ray and 2-ray models. Finally, based on the conventional two models, we propose a new algorithm for analyzing the field intensities in inhomogeneous propagation environments.

2.1 Random Allocation of Sensors

The sensor device equipped with an antenna collects many physical information such as temperature, humidity, luminous intensity and so on. Since it begins to communicate with other sensor nodes automatically, they lead to construct sensor networks. When we use sensor devices, they can be located not only in closed space but also in complicated natural environments such as dessert and sea surfaces. Then we allocate the sensor nodes appropriately to maximize their system functionality in closed space. However, we would distribute them randomly in open space by scattering those from an aircraft, for example. Therefore, it is important to analyze field intensity distribution caused by sensors in order to develop the circuit or construct optimized networks. In this paper, we estimate electric field distribution caused by sensors located randomly on terrestrial surfaces by using 1-ray and 2-ray models.

By using random variable, the allocation of sensor is given by [12]

$$l_n(x,y) = (R_x(n), R_y(n)) \quad (n = 1, 2, ..., N) \tag{1}$$

where $R_x(n)$ and $R_y(n)$ are generated by random variable as $R_x(n) \neq R_y(n)$. Fig.1 shows random allocation of sensor node generated by Eq.(1). Number of sensors is 10 in Fig.1(a) and 50 in Fig.1(b), respectively. It is shown that the sensors are located randomly in one square kilometers.

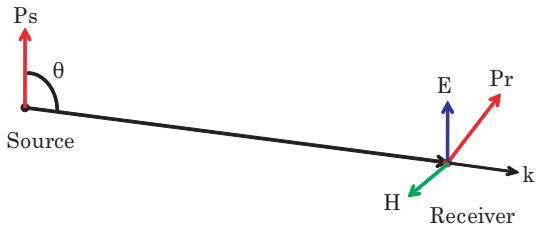

Fig. 2. Incident ray.

2.2 Incident Field

We introduce approximate solutions based on 1-ray and 2-ray models. We first review those models. 1-ray model means incident wave, and 2-ray model means the total field which includes incident wave and reflected wave from the plane-ground. Fig.2 shows the geometry of the radiation field from an antenna. $\boldsymbol{P_s}$ is a position vector of source antenna, and $\boldsymbol{P_r}$ is a position vector of receive antenna. The incident field emitted from the small dipole antenna is expressed as follows [13, 14]:

$$\boldsymbol{E_i} = \sqrt{30GP}\sin\theta\frac{e^{-j\kappa_0 r}}{r}\boldsymbol{\Theta}^v(\boldsymbol{r}, \boldsymbol{p_s}) \tag{2}$$

where the time dependence $e^{j\omega t}$ is assumed. In Fig. 2, the k-vector $\boldsymbol{k}$ denotes the direction of radiation which is perpendicular to both the incident electric field $\boldsymbol{E_i}$ and the magnetic field $\boldsymbol{H_i}$ obeying the right-hand rule. The wavelength in the free space is given by

$$\kappa_0 = \omega\sqrt{\epsilon_0\mu_0} = \frac{2\pi}{\lambda} \tag{3}$$

where λ is the wavenumber. The input power of the small dipole antenna is $P[W]$ and its absolute gain is given by G in Eq.(2). The directivity of the antenna $D(\theta) = \sin\theta$ is given by

$$\sin\theta = \frac{|\boldsymbol{p_s}\times\boldsymbol{r}|}{r}\,. \tag{4}$$

Thus the small dipole antenna exhibits the maximum radiation at $\theta = 90°$ [11]. The unit vectors of electromagnetic polarization are given by

$$\begin{aligned}\boldsymbol{\Theta}^v(\boldsymbol{r}, \boldsymbol{p_s}) &= \frac{[(\boldsymbol{r}\times\boldsymbol{p_s})\times\boldsymbol{r}]}{|(\boldsymbol{r}\times\boldsymbol{p_s})\times\boldsymbol{r}|}\\ \boldsymbol{\Theta}^h(\boldsymbol{r}, \boldsymbol{p_s}) &= \frac{(\boldsymbol{r}\times\boldsymbol{p_s})}{|\boldsymbol{r}\times\boldsymbol{p_s}|}\,.\end{aligned} \tag{5}$$

It is worthy noting that Eq.(2) behaves in the far zone from the source antenna as follows:

$$|\boldsymbol{E_i}| = O(r^{-1}) \quad (r >> \lambda)\,. \tag{6}$$

2.3 Incident and Reflected Fields

Next we discuss 2-ray model including incident wave and reflected wave from the plane-ground. Fig.3 shows the geometry of an incident ray emitted from a source antenna located above a smooth plane-ground together with its reflected ray from the plane-ground. The field expression for reflection is

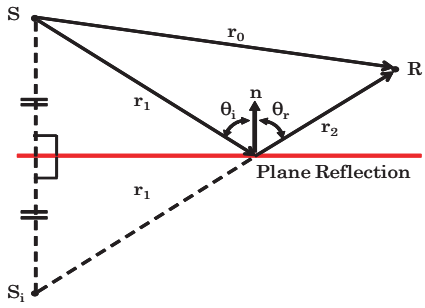

Fig. 3. Reflected ray.

given by

$$\boldsymbol{E_r} = \sqrt{30GP}\sin\theta_0 \frac{e^{-j\kappa_0 r_0}}{r_0}\boldsymbol{e_r} \tag{7}$$

where

$$r_0 = r_1 + r_2 \tag{8}$$

and

$$\sin\theta_0 = \frac{|\boldsymbol{p_s}\times\boldsymbol{r_1}|}{r_1}\,. \tag{9}$$

The electric field vector $\boldsymbol{e_r}$ which expresses reflection from the plane-ground is given by

$$\boldsymbol{e_r} = R^v(\theta_i)[\boldsymbol{\Theta}^v(\boldsymbol{r_1},\boldsymbol{p})\cdot\boldsymbol{\Theta}^v(\boldsymbol{r_1},\boldsymbol{n})]\boldsymbol{\Theta}^v(\boldsymbol{r_2},\boldsymbol{n})] + R^h(\theta_i)[\boldsymbol{\Theta}^h(\boldsymbol{r_1},\boldsymbol{p_s})\cdot\boldsymbol{\Theta}^h(\boldsymbol{r_1},\boldsymbol{n})]\boldsymbol{\Theta}^h(\boldsymbol{r_2},\boldsymbol{n})] \tag{10}$$

where $\boldsymbol{r_1}$ is a distance vector from source to reflection point, and $\boldsymbol{r_2}$ is a distance vector from reflection point to observation point. $\boldsymbol{n}$ is a normal vector.

Moreover, the unit vector related to horizontal component is defined by

$$\boldsymbol{\Theta}^h(\boldsymbol{r_1},\boldsymbol{p_s}) = \frac{(\boldsymbol{r_1}\times\boldsymbol{p_s})}{|\boldsymbol{r_1}\times\boldsymbol{p_s}|} \tag{11}$$

and the reflection coefficients for horizontal and vertical polarizations are given by

$$\begin{aligned} R^h(\theta_i) &= \frac{\cos\theta_i - \sqrt{\epsilon_c - \sin^2\theta_i}}{\cos\theta_i + \sqrt{\epsilon_c - \sin^2\theta_i}} \\ R^v(\theta_i) &= \frac{\epsilon_c\cos\theta_i - \sqrt{\epsilon_c - \sin^2\theta_i}}{\epsilon_c\cos\theta_i + \sqrt{\epsilon_c - \sin^2\theta_i}} \end{aligned} \tag{12}$$

where the incident angle θ_i can be derived from

$$\sin\theta_i = \frac{|\boldsymbol{n}\times\boldsymbol{r_1}|}{r_1}\,. \tag{13}$$

The complex dielectric constant used in Eq.(12) is defined by

$$\epsilon_c = \epsilon_r - j\frac{\sigma}{\omega\epsilon_0} \tag{14}$$

where ϵ_r and σ are dielectric constant and conductivity of the plane-ground, respectively.

In the 2-ray model, the total field at a receiving point is given by the sum of incident and reflected waves, and consequently we obtain the final field expression as follows:

$$\boldsymbol{E_t} = \boldsymbol{E_i} + \boldsymbol{E_r} = \sqrt{30GP}\sin\theta\frac{e^{-j\kappa_0 r}}{r}\boldsymbol{e_t}\ . \tag{15}$$

where the total field vector is given by

$$\boldsymbol{e_t} = \boldsymbol{\Theta}^v(\boldsymbol{r}, \boldsymbol{p_s}) + \boldsymbol{e_r}\frac{\sin\theta_0}{\sin\theta}\cdot\frac{r}{r_0}\cdot e^{-j\kappa_0(r_0-r)}\ . \tag{16}$$

It is worthy noting that the electric field above a ground plane behaves in the far zone from the source antenna as follows:

$$|\boldsymbol{E_t}| = O(r^{-2}) \quad (r >> \lambda)\ . \tag{17}$$

2.4 1-Ray and 2-ray Models

Considering the real situation, field intensity is subject to a rapid disturbance due to reflections and diffractions by dense high rise building in urban area or complicated terrestrial surfaces. It has been reported that in the urban, suburban and open areas, electric field distributions behave empirically as follows [15]:

$$|\boldsymbol{E}| = O(r^{-\beta}) \quad (r >> \lambda) \tag{18}$$

where the constant β is a distance order of propagation.

By modifying Eqs.(2) and (15), we propose two types of modal waves which behave as Eq.(18) in the far zone, and which can also simulate electromagnetic wave propagation in complicated natural environments approximately. The proposed approximations for the two models are expressed as follows:

$$\begin{aligned}\boldsymbol{E_i} &\simeq 10^{\alpha/20}\sqrt{30GP}\frac{e^{-j\kappa_0 r}}{r^\beta}\boldsymbol{\Theta}^v(\boldsymbol{r}, \boldsymbol{p_s})\\ \boldsymbol{E_r} &\simeq 10^{\alpha/20}\sqrt{30GP}\frac{e^{-j\kappa_0 r_0}}{r_0^\beta}\boldsymbol{e_r}\ .\end{aligned} \tag{19}$$

As a result, the total field is given by

$$\begin{aligned}\boldsymbol{E_t} &\simeq 10^{\alpha/20}\sqrt{30GP}\frac{e^{-j\kappa_0 r}}{r^\beta}\boldsymbol{e_t}\\ \boldsymbol{e_t} &= \boldsymbol{\Theta}^v(\boldsymbol{r}, \boldsymbol{p}) + \frac{r^\beta e^{-j\kappa(r_0-r)}}{r_0^\beta}\boldsymbol{e_r}\end{aligned} \tag{20}$$

where α is the amplitude modification, and β is the distance order of propagation [11, 12]. Eqs.(2) and (7) show $|E| \propto r^{-1}$, that is, $\beta = 1.0$ in the free space. In the complicated environment, however,

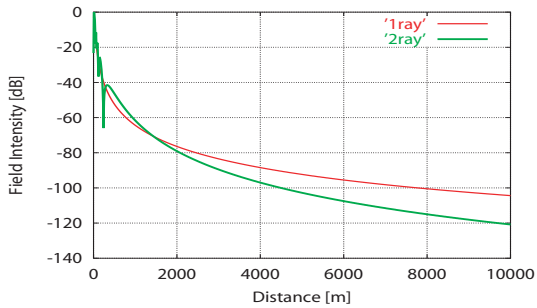

Fig. 4. 1-ray model and 2-ray model.

(a)1-ray model. (b)2-ray model.

Fig. 5. Field intensity distribution calculated by 1-ray and 2-ray models.

we have $\beta \neq 1.0$ and attenuation is enhanced as β is increased. Rewriting the total field in dB leads to the following equation:

$$|\boldsymbol{E_t}| \simeq A + \alpha - 20\beta \log_{10}(r) \ \ [\mathrm{dBV/m}] \tag{21}$$

$$A = 20 \log_{10}(\sqrt{30GP}|\boldsymbol{e_t}|) \ . \tag{22}$$

This equation is very simple, but it enables us to estimate easily the field intensity distribution in complicated propagation environments by choosing two parameters.

Fig.4 shows the field intensity distributions obtained by 1-ray and 2-ray models with $\alpha = 0[dB]$ and $\beta = 1.0$. The source height and the receiver height are chosen as 30[m] and 1.5[m], respectively. We select the following parameters; $f = 800.0[MHz]$, input power $P = 10[W]$, absolute gain G=1.5, $\epsilon_r = 5.0$ and $\sigma = 0.0023[S/m]$. In this figure, it is shown from the result of 2-ray model that some break points occur in the near field, and the field intensity of 2-ray model is more attenuate than that of 1-ray model. Figs.5(a) and 5(b) show the two dimensional (2D) field intensity distributions calculated by 1-ray and 2-ray models with $\alpha = 0[dB]$ and $\beta = 1.0$, respectively. The field areas are in one square kilo-meters.

Fig.6 shows the field intensity distributions obtained by 1-ray and 2-ray models with $\alpha = 0[dB]$. Upper two curves are the results of $\beta = 1.0$, and lower two curves are the results of $\beta = 1.5$. It is demonstrated that the larger β is, the lager field attenuation becomes.

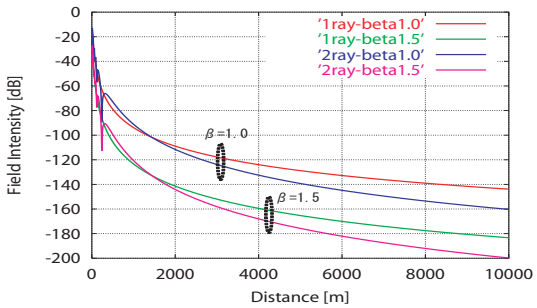

Fig. 6. 1-ray and 2-ray models with different order.

Concerning terrestrial surfaces such as dessert/sea surfaces which are assumed to be RRSs, two modification factors (α, β) depend on the shapes of RRSs which are varied by correlation length (cl) and deviation of its height (h). We have investigated the above relationship and determined two parameters (α, β) by comparing with the field distribution along RRSs computed by the DRTM. In the DRTM computation, we have used isotropic antenna with absolute gain $G = 1.0$ and input power $P = 1.0[W]$. In Table 1, we show relationship between RRS's parameters and modification factors. Since the sensors should communicate anywhere, we employ the isotropic antenna with $G = 1.0$ where we select parameters as $f = 1.0[GHz]$ and $P = 1.0[W]$. It is shown that the smaller cl is, the lager α becomes. It is also demonstrated that the larger h is, the larger α becomes. The values of β are almost same irrespective of the RRS's shapes. In the numerical examples, we use the values shown in Table 1.

Table 1. Example of relationship between RRS's parameters and modification factors (isotropic antenna).

RRS parameters		Correction values			
		1-ray model		2-ray model	
$cl[m]$	$h[m]$	$\alpha[dB]$	β	$\alpha[dB]$	β
20	5	5.0	1.45	-15.0	0.45
	10	-4.0	1.44	-24.5	0.44
	15	-9.0	1.44	-29.5	0.44
	20	-2.0	1.44	-32.5	0.44
30	5	14.0	1.45	-6.5	0.45
	10	3.0	1.45	-17.0	0.45
	15	-1.5	1.45	-22.0	0.45
	20	-6.0	1.45	-26.0	0.45
40	5	20.5	1.44	0.0	0.44
	10	10.5	1.44	-10.0	0.44
	15	5.5	1.46	-15.0	0.46
	20	2.0	1.465	-18.5	0.465

2.5 Field Estimation in Inhomogeneous Propagation Environment

Since two models described in previous subsection are applied to homogeneous propagation environment, we can not deal with the complicated field distributions directly in inhomogeneous propagation environments, such as the terrestrial surfaces consisting of the mixture of homogeneous RRSs as

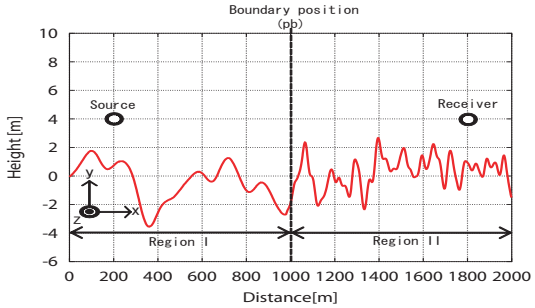

Fig. 7. Example of inhomogeneous random rough surface.

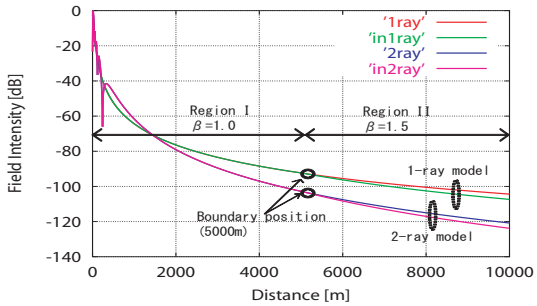

Fig. 8. One example of field intensities in inhomogeneous propagation environment.

shown in Fig.7. Therefore, we propose a field estimation method which can compute the field intensity continuously at boundary point between different propagation environments, based on 1-ray and 2-ray models. The expressions for incident wave are summarized as follows:

$$\begin{aligned} \boldsymbol{E} &\simeq \boldsymbol{E_i}(\alpha_1, \beta_1, r) \qquad (x \leq pb) \\ \boldsymbol{E} &\simeq 10^{\Gamma_b^i} \boldsymbol{E_i}(\alpha_2, \beta_2, r) \quad (x > pb) \end{aligned} \tag{23}$$

where r is a distance from source to receiver, and pb is a position of boundary. The above equation can apply to two different regions. β_1 is an order of propagation distance in Region I, and β_2 is an order of propagation distance in Region II. And Γ_b^i is matting factor for continuing the field intensity at boundary position given by

$$\Gamma_b^i = 20 \log_{10} \left(\boldsymbol{E_i}(\alpha_2, \beta_2, r') - \boldsymbol{E_i}(\alpha_1, \beta_1, r') \right) . \tag{24}$$

where r' is defined by the distance from source to boundary position. It should be noted that $\boldsymbol{E_i}$ of Eq.(23) is defined by Eq.(19).

On the other hand, the field expressions for total field of incident and reflected waves are given by

$$\begin{aligned} \boldsymbol{E} &\simeq \boldsymbol{E_t}(\alpha_1, \beta_1, r) \qquad (x \leq pb) \\ \boldsymbol{E} &\simeq 10^{\Gamma_b^t} \boldsymbol{E_t}(\alpha_2, \beta_2, r) \quad (x > pb) \end{aligned} \tag{25}$$

Total fields are defined by Eq.(20). Matting factor Γ_b^t of total field is defined by

$$\Gamma_b^t = 20 \log_{10} \left(\boldsymbol{E_t}(\alpha_2, \beta_2, r') - \boldsymbol{E_t}(\alpha_1, \beta_1, r') \right) . \tag{26}$$

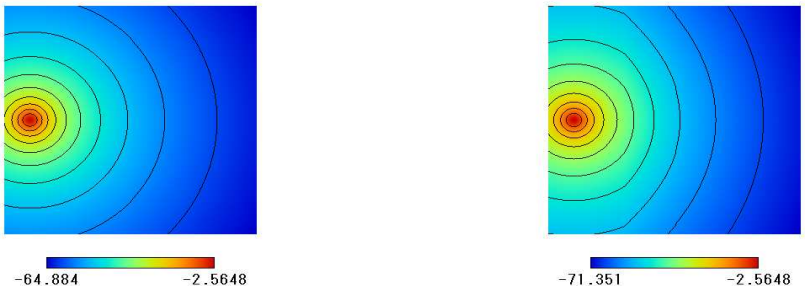

(a) Homogeneous field. (b) Inhomogeneous field.

Fig. 9. Field intensity distribution calculated by Eq.(23).

(a) Homogeneous field. (b) Inhomogeneous field.

Fig. 10. Field intensity distribution calculated by Eq.(25).

It should be noted that $\Gamma_b^t \simeq \Gamma_b^i$ in the far zone.

Fig.8 shows the field intensities calculated by Eqs.(23) and (25). Source is located at $(x, y, z) = (0, 0, 30)[m]$, and receiver is $1.5[m]$ high above the plane-ground. Propagation distance is $10,000[m]$, and the boundary is located at $x = 5,000[m]$. We select $\alpha = 0.0[dB]$ in Regions I and II, and the values of β are chosen as $\beta_1 = 1.0$ in Region I and $\beta_2 = 1.5$ in Region II, respectively. Since the value of β in Region II is larger than that of Region I, the slopes of field attenuations in Region II are larger than those in Region I. It is shown that the field intensities at boundary position are treated to be continuity.

Fig.9 shows the field intensity distributions above homogeneous and inhomogeneous propagation environments by using Eq.(23). Analytical region in these figures is in one square kilo-meter. Source point is located at $(x, y, z) = (100, 500, 30)[m]$, and receiver is located at $1.5[m]$ above a ground. From theses figures, we can see the constant attenuations in homogeneous case and attenuation changing at boundary position in inhomogeneous case. Fig.10 shows the field intensity distributions above homogeneous and inhomogeneous propagation environments by using Eq.(25). The parameters are selected as same as that of former problem. We can see some break points in these figures.

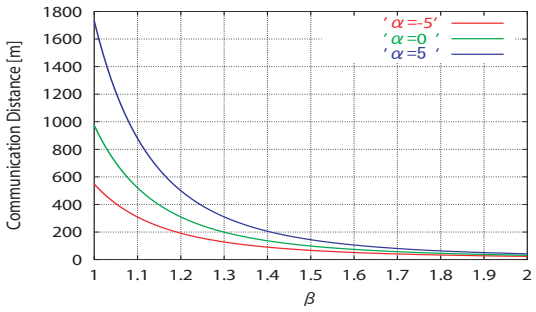

Fig. 11. Communication distance.

3 Communication Distance

In this section, we discuss an estimation method for radio communication distance based on the 1-ray and 2-ray models. From Eq.(19), electric field intensity of the 1-ray model is given by

$$|\boldsymbol{E}| = 10^{\frac{\alpha}{20}} \cdot \frac{\sqrt{30GP}}{r^{\beta}} \quad [V/m] \tag{27}$$

where the antenna orientation is assumed to be arranged so that the maximum received power can be obtained. Rewriting the above equation in dB leads to the following equation:

$$E = A + \alpha + 20\beta \log_{10} r \quad [dBV/m] \tag{28}$$

where

$$A = 20 \log_{10} \sqrt{30GP} \ . \tag{29}$$

Let E^{min} be the minimum detectable electric field intensity, then Eq.(27) yields communication distance r_c as follows [9, 10]:

$$r_c = 10^{\frac{\alpha}{20\beta}} \times \left(\frac{\sqrt{30GP}}{E_1^{min}} \right)^{\frac{1}{\beta}} \ . \tag{30}$$

We can also rewritten Eq.(28) in dB expression as follows:

$$r_c = 10^{\frac{\alpha}{20\beta}} + 10^{\frac{A - E_1^{min}}{20\beta}} \ . \tag{31}$$

The above equations are very useful for easily estimating the communicable length of wireless systems equipped antenna, such as sensor devices. In this paper, we estimate which sensors can communicate with other sensors, using Eqs.(30) or (31). Otherwise, by comparing the received power E with the minimum received power of sensor E_{min}, we judge sensors which can communicate with other sensors.

Fig.11 shows communication distance computed by Eq.(31) when β is varied with α as a parameter. We select input power as $P = 1[mW]$ and minimum received power as $E_{min} = -75[dB]$. It is shown that the larger β is, the shorter communication distance becomes. It is also demonstrated that the larger α is, the longer communication distance becomes. The proposed estimation method enables us to easily compute the radio communication distance. In this paper, we estimate the communication length of wireless device by using Eq.(31) or judging the field intensity between two devices.

(a) 10 sensors. (b) 50 sensors.

Fig. 12. Field intensity distribution caused by sensors.

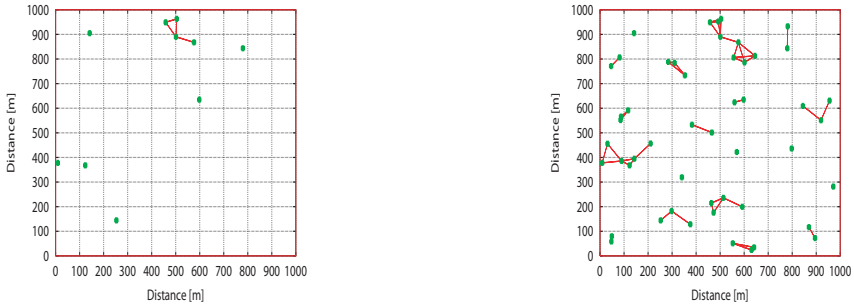

(a) 10 sensors. (b) 50 sensors.

Fig. 13. Communicable sensors above a plane-ground.

4 Numerical Example

Based on the 2-ray model, we estimate the field intensity distributions caused by sensors located on the terrestrial surfaces. The allocation of sensors are shown in Fig.1. We use following parameters: operating frequency $f = 900.0[MHz]$, input power $P = 1[mW]$, relative permittivity $\epsilon_r = 5.0$ and conductivity $\sigma = 0.0023[S/m]$. We use isotropic antenna with absolute gain $G = 1.0$ because the sensors should be communicate anywhere. We select both source and receiver heights to be 0.5[m] high above the ground.

First we consider the sensors located on the plane ground. Fig.12 shows the field intensity distributions caused by sensors distributed randomly in one square kilo-meter. Two figures are shown: (a) is the field distribution caused by 10 sensors, and (b) is the field distribution caused by 50 sensors. These numerical data are computed by using 2-ray models with $\alpha = 0.0$ and $\beta = 1.0$ as parameters. In Fig. 12(a), we can see some very low field intensities in the area. On the other hand, it is shown that field intensities in Fig. 12(b) are larger than that of Fig. 12(a) since the sensors cover the field area strongly.

Next, we consider the communicable sensors based on the field data. The minimum received sensitivity of realistic sensors are various, but we assume here the receiver sensitivity to be $E_{min} = -75[dBV/m]$) in this paper. From Fig.12, we estimate the communicable sensors. Fig.13(a) shows communicable sensors by using solid red line where we use 10 sensors. This shows that the sensor can communicate if each sensor is connected with other sensors by lines. In this case, since the field

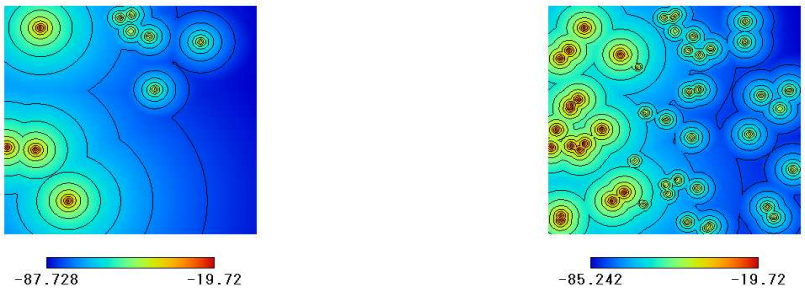

(a) 10 sensors. (b) 50 sensors.

Fig. 14. Field intensity distribution caused by sensors in inhomogeneous propagation environment.

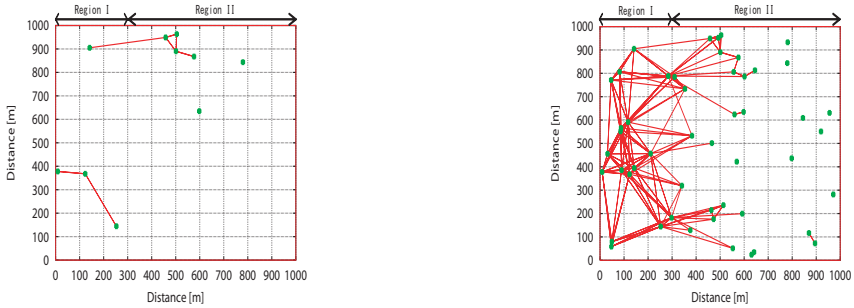

(a) 10 sensors. (b) 50 sensors.

Fig. 15. Communicable sensors in inhomogeneous propagation environment.

intensities are very small, the sensors cannot construct networks. It is shown that only four sensors among 10 sensors are communicated with each other. Fig.13(b) shows communicable sensors by using solid red line where we scatter 50 sensors. It is shown that the sensors can construct some networks due to the more sensors distributed than that of Fig.13(a). However, it is difficult to mention that sensors construct enough networks in order to gather the physical data. As a result, it is found that we need more sensors than above examples to construct networks in this case.

Plane-ground is a kind of homogeneous propagation environment. Consequently, the field intensities are computed by basic 2-ray model. Considering the realistic environments, there are very complicated terrestrial surfaces such as random rough surface. In order to compute the field intensity distribution above RRS, we need to employ numerical methods, such as FDTD/FVTD, Kirchhoff approximation and DRTM. These methods are so useful to analyze the behaves of electromagnetic wave, but they require much computation time or computer memory. Therefore we have proposed 1-ray and 2-ray models employing amplitude modification (α) and order of propagation distance (β), and we have shown that two models can approximately express the field intensities above RRSs. In addition, by using Eqs.(30) and (31), we have considered how many sensor nodes are needed to construct networks. In that study, we have only analyzed the field intensity distribution in homogeneous propagation environment. Therefore, we analyze the field intensity distribution and communicable sensors in inhomogeneous environment by using Eq.(25).

Fig.14 shows the field intensity distributions in inhomogeneous propagation environment. This

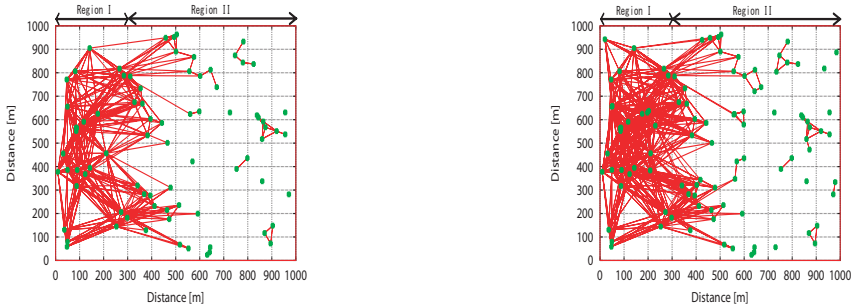

(a) 80 sensors. (b) 100 sensors.

Fig. 16. Communicable sensors in inhomogeneous propagation environment.

analytical region is in one square kilo-meter and the space is divided into two parts: one is in the region from $x = 0[m]$ to $x = 300[m]$, and the other is in the region from $x = 300[m]$ to $x = 1,000[m]$. We name the former region as Region I and the latter region as Region II. In Region I, we choose $\alpha = -6.5$ and $\beta = 0.45$. We also choose $\alpha = -24.5$ and $\beta = 0.44$ in Region II. It is found from these parameters that the propagation environment in Region II is worth than that of Region I. Figs.14(a) and (b) show the field distributions caused by 10 and 50 sensors, respectively. It is shown that the field intensities in Region I are larger than those of Region II. Boundary point is at $x = 300[m]$, but it is shown that field intensities are computed continuously. It is demonstrated that the field intensities in Fig.14(b) are larger than that of Fig.14(a) due to more sensors distributed.

Fig.15 shows the communicable sensors by using solid red line. In case that the number of sensors is a few, the communication in arbitrary area is not established well. We can see large networks established in the arbitrary area when we distribute 50 sensors. However, sensor nodes located in Region II can not construct networks due to small field intensity.

Next, we consider the number of sensors in arbitrary area. We have so far selected the area size to be one square kilo-meter, and have distributed 10 and 50 sensors. When the number of sensors is 10, it has been inadequate to construct networks. Even if we distribute 50 sensors, they cannot construct the networks perfectly when the field intensity is very small. Due to this reason, we need to distribute more sensor nodes in the region where the field intensity distributions are very small. Fig. 16 shows the communicable sensors by using solid red line. Fig. 16(a) shows the communicable sensors where the 80 sensors are distributed, and Fig. 16(b) shows the communicable sensors where the 100 sensors are distributed. We can see small networks in Region II since the number of sensors are increaser than those in the previous figures. It is also shown that the distributed sensors can construct enough network in Region I.

Finally, we show another inhomogeneous problem as shown in Fig.17. The space is divided into three parts, and we choose the following parameters; $\alpha = -15.0[dB]$ and $\beta = 0.45$ in Region I, $\alpha = -17.0[dB]$ and $\beta = 0.45$ in Region II, $\alpha = -10.0[dB]$ and $\beta = 0.44$ in Region III. We have determined these parameters from the results of Table 1. Fig.18 shows the field intensity distributions in inhomogeneous propagation environment. Fig.18(a) is the field intensity distribution caused by 10 sensors, and Fig.18(b) is the field intensity distribution caused by 50 sensors. Base on these field data, the communicable sensors are shown in Fig.19. We can see large networks in Fig.18(b).

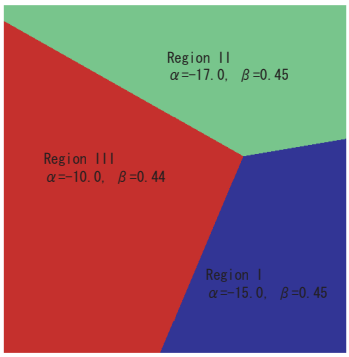

Fig. 17. Geometry of the problem.

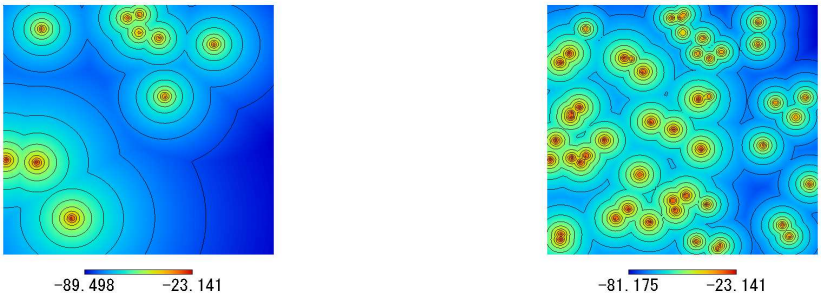

(a) 10 sensors. (b) 50 sensors.

Fig. 18. Field intensity distributions caused by sensors in inhomogeneous propagation environment.

5 Conclusion

In this paper, we have investigated the field intensity distribution caused by sensors located randomly on inhomogeneous terrestrial surfaces, and have considered the number of sensors in arbitrary areas in order to construct networks.

First we have introduced the allocation algorithm for sensors based on the random variation. Next, we have proposed the field estimations of electromagnetic waves based on 1-ray and 2-ray models with two modification factors which are the amplitude modification (α) and the distance order of propagation (β). By using the two factors, we can treat flexibly the field intensity distribution in complicated propagation environments. In addition, based on proposed 1-ray and 2-ray models, we have proposed an estimation formula for analyzing electric field intensity in inhomogeneous propagation environments. The numerical results have shown the field intensity distributions depending on the number of sensors. It has been shown that the more number of sensors is, the larger the field intensity distribution becomes.

Finally, we have introduced the estimation algorithm for radio communication distance based on 1-ray and 2-ray models. This enables us to estimate communication distance of wireless devices easily when we simply set the input power of antenna and receiver sensitivity. In the numerical examples, we have shown the field intensity distribution caused by sensors distributed randomly on inhomogeneous terrestrial surfaces by employing α and β estimated. We have also shown the communicable distance

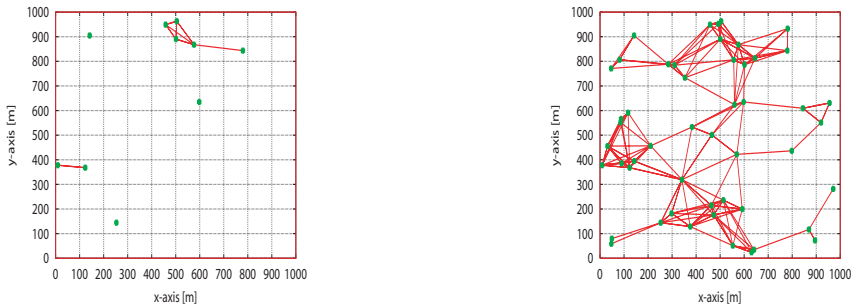

(a) 10 sensors. (b) 50 sensors.

Fig. 19. Communicable sensors in inhomogeneous propagation environment.

of each sensor, and have discussed which sensor communicates with other sensors. As a result, a few sensors cannot construct enough networks to collect information. In order to construct enough networks, we need the moderate number of sensors or more.

In this paper, we have considered the sensor network from a view point of the physical layer of OSI model. Considering not only the physical layer but also network layer, we would like to investigate the optimized allocation of sensors and the circuit of sensor devices. These will be our future work.

References

1. D.B. Lowe and J. Eklund (2002), *Client needs and the design process in Web projects*, J. Web Engineering, Vol.1, pp. 023-036.
2. Y. Tobe (2007), *Trend of Technologies in Wireless Sensor Networks*, *IEICE Trans. Commun.,* Vol. J90-B, No.8, pp. 711-719.
3. I. F. Akyildiz, I. H. Kasimoglu (2004), *Wireless sensor and actor networks: research challenges*, *Ad Hoc Networks Journal (Elsevier),* 2(4), pp.351-367.
4. O. Younis, S. Fahmy (2004), *HEED: A hybrid, energy-efficient, distributed clustering approach for ad-hoc sensor networks, IEEE Transaction on Mobile Computing,* 3(4), pp.366-379.
5. K. Uchida, H. Fujii, M. Nakagawa, X.F. Li and H. Maeda (2007), *FVTD Analysis of Electromagnetic Wave Propagation along Rough Surface*, *IEICE Trans. Commun.,* Vol. J90-B, No. 1, pp. 48-55.
6. K.S. Yee (1966) *Numerical solution of initial boundary value problems involving Maxwell's equation*, *IEEE Trans. Antennas Propag.*, Vol. 14, No. 3, pp. 302-307.
7. E.I. Thoros (1988) *The validity of the Kirchhoff approximation for rough surface scattering using a Gaussian roughness spectrum*, *J. Acoust. Soc. Am.,* Vol. 83, No. 1, pp. 78-92.
8. E.I. Thoros (1988) *The validity of the perturbation approximation for rough surface scattering using a Gaussian roughness spectrum*, *J. Acoust. Soc. Am.,* Vol. 86, No. 1, pp. 261-277.
9. K. Uchida and J. Honda (2010) Estimation on Radio Communication Distance and Propagation Characteristics along Random Rough Surface for Sensor Networks, Wireless Sensor Networks: Application-Centric Design, Geoff V Merret and Yen Kheng Tan (Ed.), InTech, Chapter 13, pp. 231-248.
10. J. Honda, K. Uchida and K.Y. Yoon (2010) *Estimation of Radio Communication Distance along Random Rough Surface*, *IEICE Trans. Electron.,* Vol. E93-C, No. 1, pp. 39-45.
11. K. Uchida, J. Honda, T. Tamaki and M. Takematsu (2011) *Handover Simulation based on a Two-Rays Ground Reflection Model*, Proceedings of The 2011 International Conference on Complex, Intelligent, and Software Intensive Systems, pp. 414-419.
12. J. Honda and K. Uchida (2011) *Analysis of Field Distribution and Density of Sensor Node*, *Proceedings of the IEEE International Conference on Intelligent Networking and Collaborative System,* pp. 122-129.
13. Yasuto Mushiake (1985) Antennas and Radio Propagation, *Corona Publishing Co., LTD. Tokyo.*
14. Robert E. Collin (1985) Antennas and Radiowave Propagation, *McGraw-Hill Book Company, New York.*

15. M. Hata (1980) *Empirical Formula for Propagation Loss in Land Mobile Radio Services, IEEE Trans. Veh. Technol.*, vol. VT-29, no.3, pp.317-325.